TPC2 polymorphisms associated with a hair pigmentation phenotype in humans result in gain of channel function by independent mechanisms

Yu-Kai Chao[a,1], Verena Schludi[a,1], Cheng-Chang Chen[a], Elisabeth Butz[a], O. N. Phuong Nguyen[a], Martin Müller[a], Jens Krüger[b], Claudia Kammerbauer[c], Manu Ben-Johny[d], Angelika M. Vollmar[a], Carola Berking[c], Martin Biel[a], Christian A. Wahl-Schott[a,2], and Christian Grimm[a,2]

[a]Department of Pharmacy, Center for Drug Research and Center for Integrated Protein Science Munich, Ludwig-Maximilians-Universität München, 81377 Munich, Germany; [b]High-Performance and Cloud Computing Group, Zentrum für Datenverarbeitung, Universität Tübingen, 72076 Tübingen, Germany; [c]Department of Dermatology, Medical Faculty, Ludwig-Maximilians-Universität München, 80337 Munich, Germany; and [d]Calcium Signals Laboratory, Department of Biomedical Engineering, The Johns Hopkins University School of Medicine, Baltimore, MD 21205

Edited by Dejian Ren, University of Pennsylvania, Philadelphia, PA, and accepted by Editorial Board Member David E. Clapham August 16, 2017 (received for review April 6, 2017)

Two-pore channels (TPCs) are endolysosomal cation channels. Two members exist in humans, TPC1 and TPC2. Functional roles associated with the ubiquitously expressed TPCs include VEGF-induced neoangiogenesis, LDL-cholesterol trafficking and degradation, physical endurance under fasting conditions, autophagy regulation, the acrosome reaction in sperm, cancer cell migration, and intracellular trafficking of pathogens such as Ebola virus or bacterial toxins (e.g., cholera toxin). In a genome-wide association study for variants associated with human pigmentation characteristics two coding variants of TPC2, rs35264875 (encoding M484L) and rs3829241 (encoding G734E), have been found to be associated with a shift from brown to blond hair color. In two recent follow-up studies a role for TPC2 in pigmentation has been further confirmed. However, these human polymorphic variants have not been functionally characterized until now. The development of endolysosomal patch-clamp techniques has made it possible to investigate directly ion channel activities and characteristics in isolated endolysosomal organelles. We applied this technique here to scrutinize channel characteristics of the polymorphic TPC2 variants in direct comparison with WT. We found that both polymorphisms lead to a gain of channel function by independent mechanisms. We next conducted a clinical study with more than 100 blond- and brown/black-haired individuals. We performed a genotype/phenotype analysis and subsequently isolated fibroblasts from WT and polymorphic variant carriers for endolysosomal patch-clamp experimentation to confirm key in vitro findings.

TPC | TPC2 | two-pore channel | polymorphism | pigmentation

Two-pore channels (TPCs) are endolysosomal cation channels which are distantly related to the endolysosomal TRP channels of the TRPML subfamily on the one hand and the voltage-gated calcium channels on the other hand. Two members exist in humans, TPC1 and TPC2. Functional roles associated with the ubiquitously expressed TPCs include VEGF-induced neoangiogenesis (1), endolysosomal LDL-cholesterol trafficking and degradation (2), physical endurance under fasting conditions (3), autophagy regulation (4, 5), the acrosome reaction in sperm (6), intracellular trafficking of certain pathogens such as filoviridae (e.g., Ebola or Marburg virus) (7), bacterial toxins (e.g., cholera toxin) (8), and a role in cancer cell migration (9). A few years ago, Sulem et al. (10) presented results from a genome-wide association study for variants associated with human pigmentation characteristics among 5,130 Icelanders, with follow-up analyses in 2,116 Icelanders and 1,214 Dutch individuals from which they claimed that two coding variants of hTPC2 (SNPs), rs35264875 (encoding M484L) and rs3829241 (encoding G734E), were associated with a shift from brown to blond hair color. Very recently, Ambrosio et al. (11) as well as Bellono et al. (12) confirmed a role for TPC2 in pigmentation by showing that TPC2 regulates the pH and size of melanosomes, thus controlling the amount of melanin produced. Consequently, loss of TPC2 activity by knockout or knockdown leads to a strong increase of melanin production and melanosomal pH.

Hence, it seemed intriguing to functionally investigate these polymorphic TPC2 variants. We investigated the activity of WT hTPC2 side by side with hTPC2(G734E) and hTPC2(M484L) as well as the double-mutant isoform (M484L/G734E). First, we applied the endolysosomal patch-clamp technique in combination with small-molecule activators and blockers of TPC2 to directly assess channel activity. Second, we performed molecular dynamics simulations of TPC2 based on the recently published structures of TPC1 (13, 14) to investigate structural changes due to the SNPs. These results were corroborated by ion substitution experiments to assess pore sizes. Furthermore, we genotyped more than 100 blond- and brown/black-haired human individuals and isolated fibroblasts from selected donors to confirm key in vitro findings and the results of the genome-wide association study by Sulem et al. (10).

Significance

Polymorphisms in the endolysosomal cation channel TPC2 have been suggested to lead to a shift in human hair color from brown to blond. In two further studies a role for TPC2 in melanosomal pH regulation was postulated. Electrophysiological data on how these polymorphisms affect channel gating and activity are, however, missing. We show here that both polymorphisms lead to a gain of channel function by different mechanisms. In M484L sensitivity to its endogenous ligand $PI(3,5)P_2$ is strongly increased while in G734E channel inactivation by ATP is reduced. These findings are corroborated by molecular dynamics and ion substitution experiments. Furthermore, >100 blond- and brown/black-haired human individuals were genotyped and fibroblasts isolated from selected donors to confirm key in vitro findings.

Author contributions: Y.-K.C., V.S., C.-C.C., E.B., O.N.P.N., J.K., A.M.V., C.B., and C.G. designed research; Y.-K.C., V.S., C.-C.C., E.B., O.N.P.N., M.M., J.K., C.K., C.B., and C.G. performed research; Y.-K.C., V.S., C.-C.C., E.B., O.N.P.N., M.M., J.K., M.B.-J., and C.G. analyzed data; and M.B., C.A.W.-S., and C.G. wrote the paper.

The authors declare no conflict of interest.

This article is a PNAS Direct Submission. D.R. is a guest editor invited by the Editorial Board.

[1]Y.-K.C. and V.S. contributed equally to this work.

[2]To whom correspondence may be addressed. Email: christian.wahl@cup.uni-muenchen.de or christian.grimm@cup.uni-muenchen.de.

This article contains supporting information online at www.pnas.org/lookup/suppl/doi:10.1073/pnas.1705739114/-/DCSupplemental.

Results

Human TPC2 WT and Polymorphic Variants Show Comparable Subcellular Distribution but Differences in Basal Activity and Their Response to PI(3,5)P_2. WT hTPC2 and the polymorphic variants containing either M484L, G734E, or both M484L and G734E show similar subcellular distribution when overexpressed in HEK293 cells (*SI Appendix*, Fig. S1*A*). All variants localize to intracellular vesicular structures which are positively stained with Lysotracker (*SI Appendix*, Fig. S1*A*). A calculation of the Pearson correlation coefficients resulted in similar numbers for colocalization with Lysotracker for all variants (*SI Appendix*, Fig. S1*B*). Western blot analysis demonstrated that expression levels of the different variants in endolysosomal membranes are not significantly different (*SI Appendix*, Fig. S1 *C* and *D*). Treatment with vacuolin increased the size of endolysosomal vesicles to a similar extent in all variants (*SI Appendix*, Fig. S1*E*). Finally, dimerization efficiencies of TPC2 WT and the polymorphic variants were comparable as assessed by FRET experimentation (*SI Appendix*, Fig. S2).

The two polymorphisms are found in very different parts of the protein. While M484L resides in the second transmembrane domain of the second channel domain, G734E is found in the C terminus of the protein (Fig. 1*A*), suggesting different functional consequences.

We next performed endolysosomal patch-clamp experiments. Here, we found striking differences between the respective variants. The polymorphic variant M484L as well as the double-polymorphic variant showed, compared with WT, a significantly increased basal channel activity as well as a significantly increased channel activity after stimulation with PI(3,5)P_2 (3, 15). In contrast, G734E showed mean basal and stimulated activation levels similar to those of WT (Fig. 1 *B*–*F* and *SI Appendix*, Fig. S3*A*). Average capacitance values were comparable for all variants, indicating that differences in channel activity were not due to differences in the size of the patched vesicles (*SI Appendix*, Fig. S3*B*). Dose–response measurements revealed an EC_{50} of 1,138 ± 376 nM for WT compared with 216 ± 55 nM for M484L, while G734E was not significantly different from WT with an EC_{50} of 827 ± 183 nM (Fig. 1*G*; increased potency). In addition, the maximum response level was increased by two- to threefold, depending on the PI(3,5)P_2 concentration, in M484L compared with WT or G734E (Fig. 1*G*; increased efficacy).

Differences in ATP Inhibition Between TPC2 WT and Polymorphic Variants. We next assessed the inhibition of activated TPC2 WT and polymorphic variants by ATP. Block of TPC activity by ATP has been demonstrated before and was shown to be physiologically relevant during cell starvation (3). We confirm here that the channel activities of WT TPC2 and also the polymorphic variants M484L and G734E are efficiently blocked by applying high concentrations of ATP (1 mM). However, dose–response measurements revealed significant differences in the IC_{50} values which were generated for each variant based on their individual PI(3,5)P_2 EC_{50} values (Fig. 2). When we used the individual PI(3,5)P_2 EC_{50} values to activate we obtained the following IC_{50} values for the ATP block: WT (91 ± 19 μM), G734E (351 ± 37 μM), and M484L (102 ± 6 μM). These data demonstrate that significantly less ATP is necessary to block WT TPC2 or M484L variant activities compared with the G734E variant. Similar results were obtained when we used the individual PI(3,5)P_2 EC_{80} values or a fixed concentration of 1 μM PI(3,5)P_2 to activate. The respective IC_{50} values for the ATP block were as follows: WT (179 ± 15 μM) and G734E (384 ± 39 μM) for PI(3,5)P_2 EC_{80} as

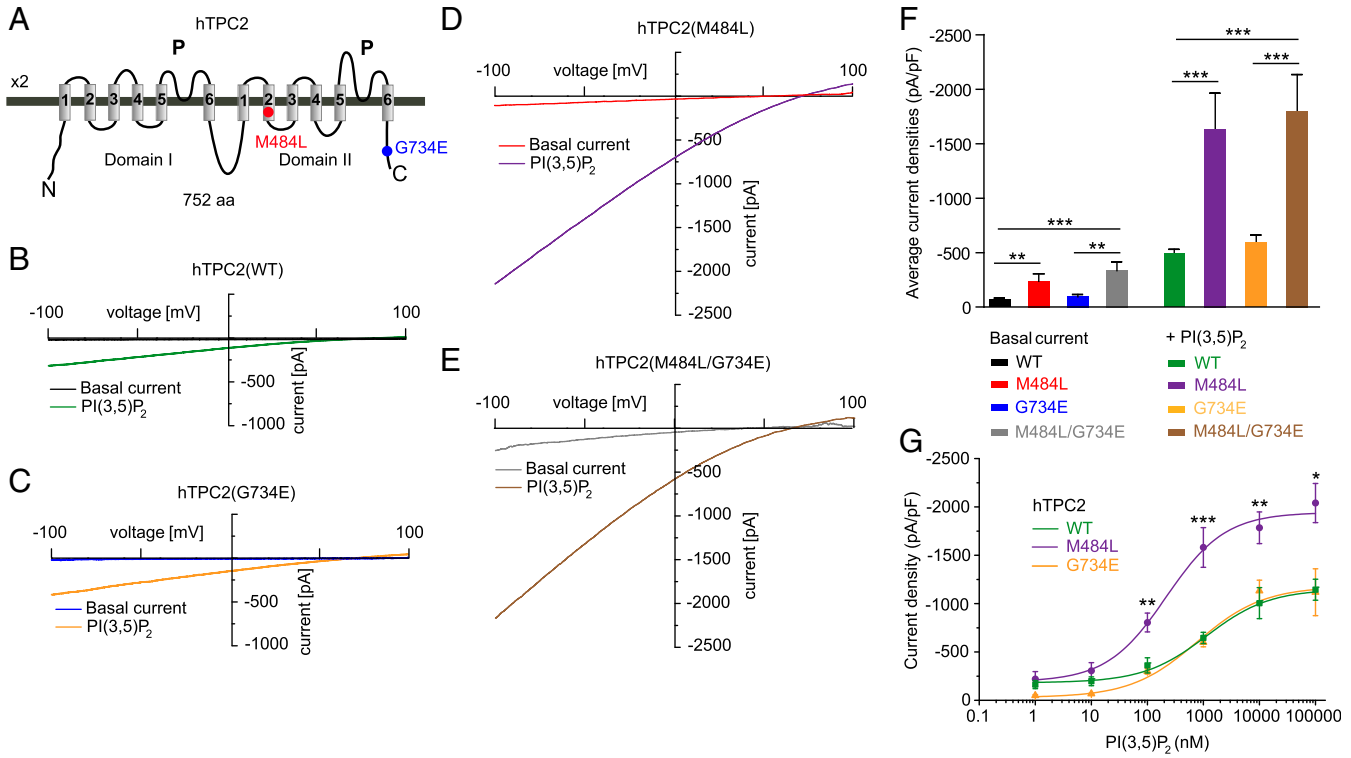

Fig. 1. Effect of PI(3,5)P_2 on endolysosomal vesicles expressing either human TPC2 WT or polymorphic variants. (*A*) Cartoon showing the estimated positions of the polymorphisms (SNPs) M484L and G734E. (*B*–*E*) Shown are representative basal and PI(3,5)P_2 (1 μM) activated currents in vacuolin-enlarged endolysosomal vesicles expressing either hTPC2 WT, hTPC2(M484L), hTPC2(G734E), or hTPC2(M484L/G734E) C-terminally fused to YFP. (*F*) Statistical summary of data as shown in *B*–*E*. Shown are average current densities at −100 mV. (*G*) PI(3,5)P_2 dose–response curves for hTPC2 WT and hTPC2(M484L) and hTPC2(G734E). In all experiments, currents were elicited by applying 500-ms voltage ramps from −100 to +100 mV every 5 s. In all statistical analyses mean values of at least 5–10 independent experiments are shown, each. To test for statistical significance the one-way ANOVA test followed by Tukey's posttest was applied. ***$P < 0.001$, **$P < 0.01$.

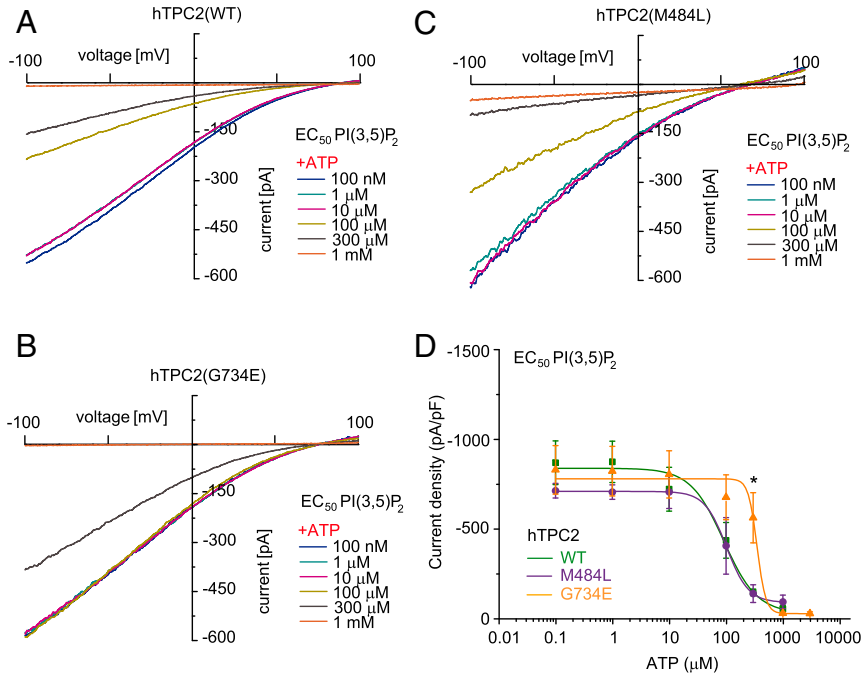

Fig. 2. Effect of ATP on human TPC2 WT and polymorphic variants using the respective EC_{50} values of $PI(3,5)P_2$ as activating concentrations. (*A*–*C*) Representative $PI(3,5)P_2$ (diC8) activated currents in vacuolin-enlarged hTPC2 WT and hTPC2 SNP expressing endolysosomal vesicles using the respective EC_{50} values as activating $PI(3,5)P_2$ concentrations and different concentrations of ATP as indicated to block the currents. (*D*) ATP dose–response curves from experiments as shown in *A*–*C*. In all experiments currents were elicited by applying 500-ms voltage ramps from −100 to +100 mV every 5 s. To test for statistical significance the Student's *t* test, unpaired was applied. $*P < 0.05$.

well as WT (4 ± 2 μM) and G734E (133 ± 71 μM) for the fixed concentration of 1 μM $PI(3,5)P_2$ (*SI Appendix*, Fig. S4).

In summary, these data suggest that both M484L and G734E variants are gain-of-function (GOF) polymorphisms.

Effect of mTOR Inhibitors. ATP is known to activate mTOR (mechanistic target of rapamycin) (16) and mTOR is the mediator that inhibits TPC2 by direct protein–protein interaction, as recently shown (3). To further investigate the cross-talk between channel activity and ATP inhibition, we tested the effect of mTOR inhibitors such as rapamycin and torin-1 on TPC2 channel activity. Both compounds were found previously to enhance TPC2 channel activity by blocking the TPC2 inhibitor mTOR (3). We found that inhibition of mTOR increased TPC2(G734E) channel activity more efficiently than WT activity, suggesting a stronger effect of mTOR on WT compared with G734E. In contrast, the channel activity of the M484L isoform could not be further enhanced under the same conditions [for M484L a $PI(3,5)P_2$ concentration of 1 μM is a saturating concentration; EC_{50} = 216 ± 55 nM] (Fig. 3 and *SI Appendix*, Fig. S5 *A* and *B*).

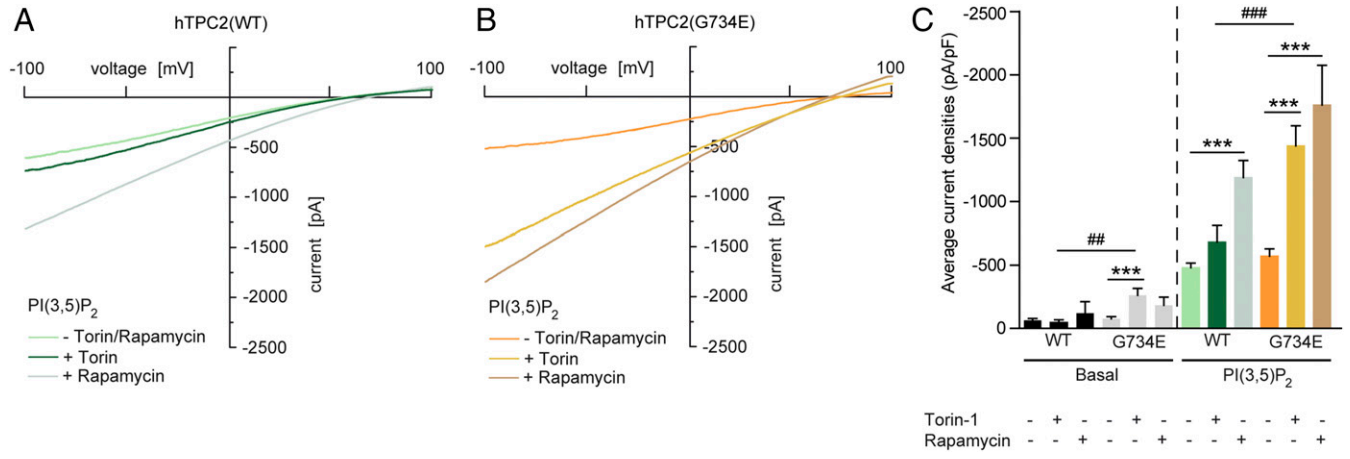

Fig. 3. Effect of rapamycin and torin-1 on human TPC2 WT and G734E. (*A* and *B*) Representative $PI(3,5)P_2$ (1 μM) activated currents in vacuolin-enlarged hTPC2 WT and hTPC2(G734E) expressing endolysosomal vesicles and the respective blocking effects of 2 μM torin-1 or 1 μM rapamycin. Cells were incubated with torin-1 for 12 h or with rapamycin for 10 min before experimentation. Currents were measured in the absence of ATP. (*C*) Statistical summary of data as shown in *A* and *B* including respective basal currents. Shown are average current densities at −100 mV. To test for statistical significance the one-way ANOVA test followed by Tukey's posttest was applied to basal and $PI(3,5)P_2$ conditions, respectively. ***, $^{###}P < 0.001$, $^{##}P < 0.01$.

Ion Substitution Experiments. To further corroborate the findings obtained for the M484L variant we performed ion substitution experiments and molecular dynamics simulations based on the recently published structures of AtTPC1 (13, 14). In ion substitution experiments using the endolysosomal patch-clamp technique we found differences in the estimated pore diameters between WT and M484L, while there were no obvious differences between WT and G734E (Fig. 4 *A–E* and *SI Appendix*, Fig. S5 *C–E*). We used monovalent cations (sodium, lithium, rubidium, and cesium) in a concentration of 160 mM, each, to estimate the pore diameters of TPC2 WT and the M484L variant (Fig. 4 *A–E*). We determined permeability ratios relative to Na^+ (P_X/P_{Na}) from the bionic reversal potentials, which resulted in estimations of 3.7 Å and 3.9 Å for the minimum pore diameter of TPC2 WT and the M484L variant, respectively. The estimation for the G734E variant diameter resulted in the same value as for WT (3.7 Å) (*SI Appendix*, Fig. 5*E*). These data suggest that M484L not only contributes to larger current amplitudes but also influences channel conformation and the narrowest part of the pore region.

Molecular Dynamics Simulations Confirm Dilated Pore in hTPC2(M484L) Variant. Multiple models of the TPC2 channel were submitted to prolonged molecular dynamics simulations of at least 100 ns, each. WT and M484L variant were simulated with $PI(3,5)P_2$ resembling the experimental layout. As each simulation system contained two channel models a total of over 800 ns was available for analysis. All models showed a high degree of stability preserving their overall structure and a continuous water column through the pore. For one of the two M484L models a dilation of the pore could be observed in the presence of $PI(3,5)P_2$ for ~10 ns around position A272. The pore radii of the dilated M484L pore were compared with the WT pore (Fig. 4 *F–H*). This finding suggests that the M484L mutation affects pore dynamics, further corroborating the data presented on the estimation of the pore sizes of TPC2 WT and M484L by ion substitution experimentation. Notably, Schieder et al. (17) had reported previously that TPC2 mutant isoform N273A (next to A272) shows a pore block, and Wang et al. (15) reported that the D276K mutation likewise leads to a pore block and loss of $PI(3,5)P_2$ response, emphasizing the importance of this region for channel activity.

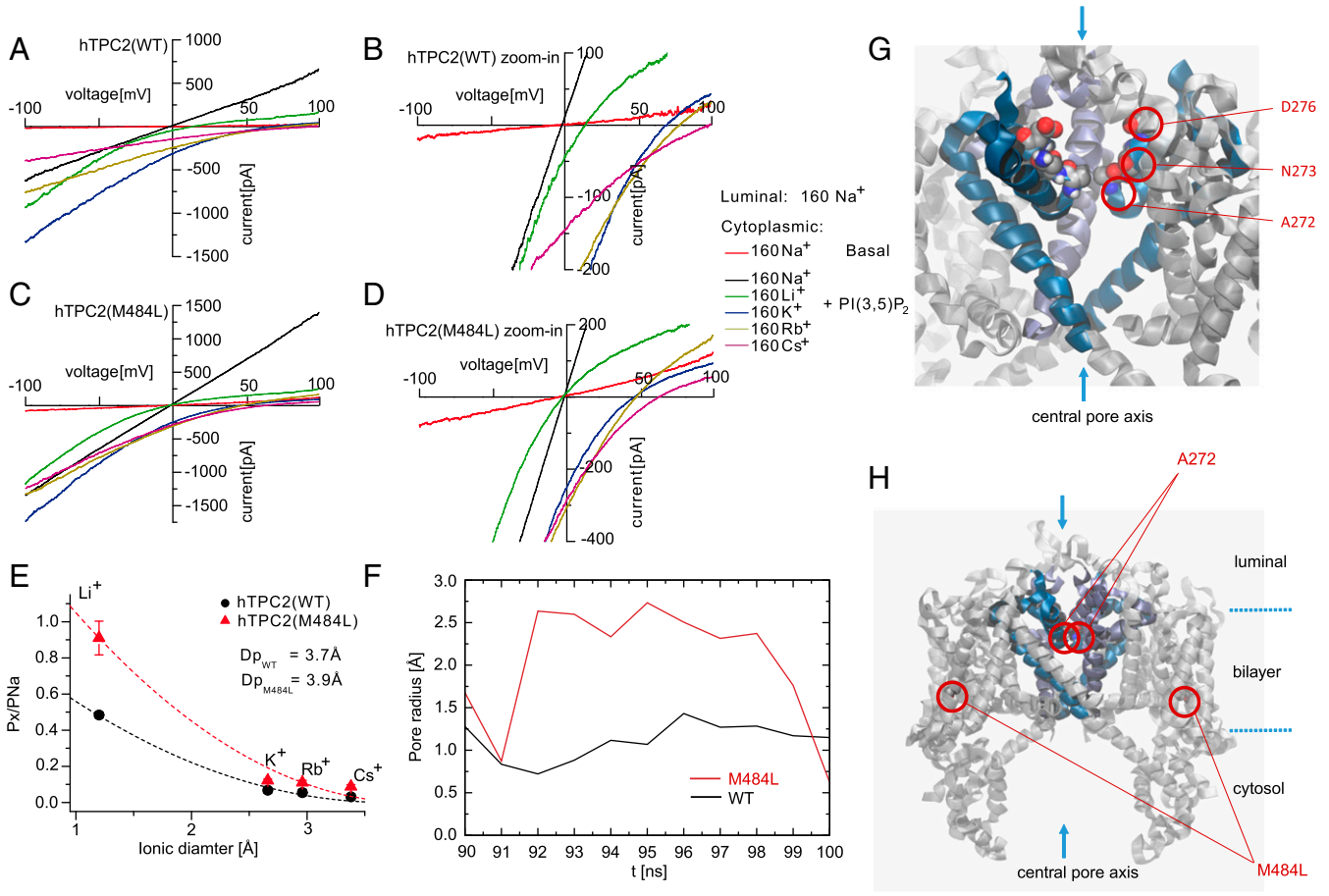

Fig. 4. Ion substitution experiments and molecular dynamics simulations. (*A–D*) Endolysosomal patch-clamp experiments showing $PI(3,5)P_2$-activated hTPC2 WT (*A* and *B*) or hTPC2(M484L) (*C* and *D*) currents under biionic conditions with luminal Na^+ and bath solutions containing the following monovalent cations, respectively: Li^+, K^+, Rb^+, and Cs^+. (*B* and *D*) Expanded view of *A* and *C*, showing that the reversal potentials are shifted to negative voltage in M484L variant. (*E*) Summary of data as shown in *A–D*. Shown are the relative permeabilities (P_X/P_{Na}) of the different cations plotted against the diameter of cations. The dashed lines are fitted to Eq. **2** (see *Materials and Methods* for details). (*F*) Schematic representation of the TPC2 simulation system. The channel (gray) is embedded in a fully solvated POPC bilayer (transparent surfaces). As the channel has a conic shape the bilayer is bent locally. To cope with this effect always two channel models were embedded in antiparallel fashion into a larger bilayer patch. (*G*) Enlargement of the selectivity filter omitting part of the protein. D276, N273, and A272, which are present symmetrically on both subunits, are shown in VdW representation. (*H*) The pore radius of TPC2 is shown at the height of A272 for WT (blue) and the M484L variant (red) simulated in presence of $PI(3,5)P_2$. A representative window at the end of the independent simulations was chosen which presumably resembles an opening event. One of two M484L pores showed a dilation of more than 1 Å for almost 10 ns.

Endogenous TPC2 Channel Activity in Human Donor Fibroblasts. Next, we screened more than 100 blond- and brown/black-haired human donors for TPC2 polymorphisms and identified individuals which were either homozygous for WT, M484L, or G734E, or individuals which were heterozygous for the respective polymorphisms (Fig. 5 *A* and *B*). The obtained genotyping results were found to correlate well with the data published by Sulem et al. (10). Thus, the percentage of DNA samples isolated from blond-haired individuals which are homozygous for either M484L or G734E was 7.2% and 26.1% ($n = 69$), respectively, while DNA samples isolated from brown-, dark brown-, or black-haired individuals were in only 2.9% of the cases homozygous for M484L and in only 10.4% of the cases homozygous for G734E ($n = 67$). Among the blond-haired donors we found only 5.8% to be homozygous for WT. Among individuals with brown/black hair 23.9% were found to be homozygous for WT (Fig. 5*A*).

We subsequently isolated fibroblasts from selected individuals and analyzed them using the endolysosomal patch-clamp technique (Fig. 5 *C*–*F*). While we found only small endogenous $PI(3,5)P_2$ currents in WT or G734E fibroblast endolysosomes, significantly increased $PI(3,5)P_2$-mediated channel activity was detectable in endolysosomes isolated from donor fibroblasts homozygous for M484L, essentially confirming the in vitro findings. For ATP dose–response measurements the $PI(3,5)P_2$-mediated currents in G734E endolysosomes were too small. As an activation control we used the TRPML-channel activator ML-SA1 (18). TRPML channel currents activated with ML-SA1 were not significantly different between M484L, G734E, and WT endolysosomes, suggesting that the differences in $PI(3,5)P_2$ response are not due to differences in TRPML channel activity (Fig. 5 *C*–*E*). In summary, these data confirm the strong GOF found for the M484L variant in overexpressing HEK293 cells and the data further confirm the increased association of the M484L and G734E variants with blond hair color compared with the WT TPC2 isoform.

Discussion

We show here that the TPC2 variants M484L and G734E reported previously to be associated with a shift in human hair color from brown to blond display distinct functional differences compared with WT. We used overexpressing HEK293 cells and endogenously expressing fibroblasts to functionally characterize the respective variants. In endolysosomal patch-clamp experiments we found that both variants show a gain of channel function compared with WT (*SI Appendix*, Fig. S6). While basal activity and activation with PI(3,5)P_2 was increased in M484L, affecting both efficacy and

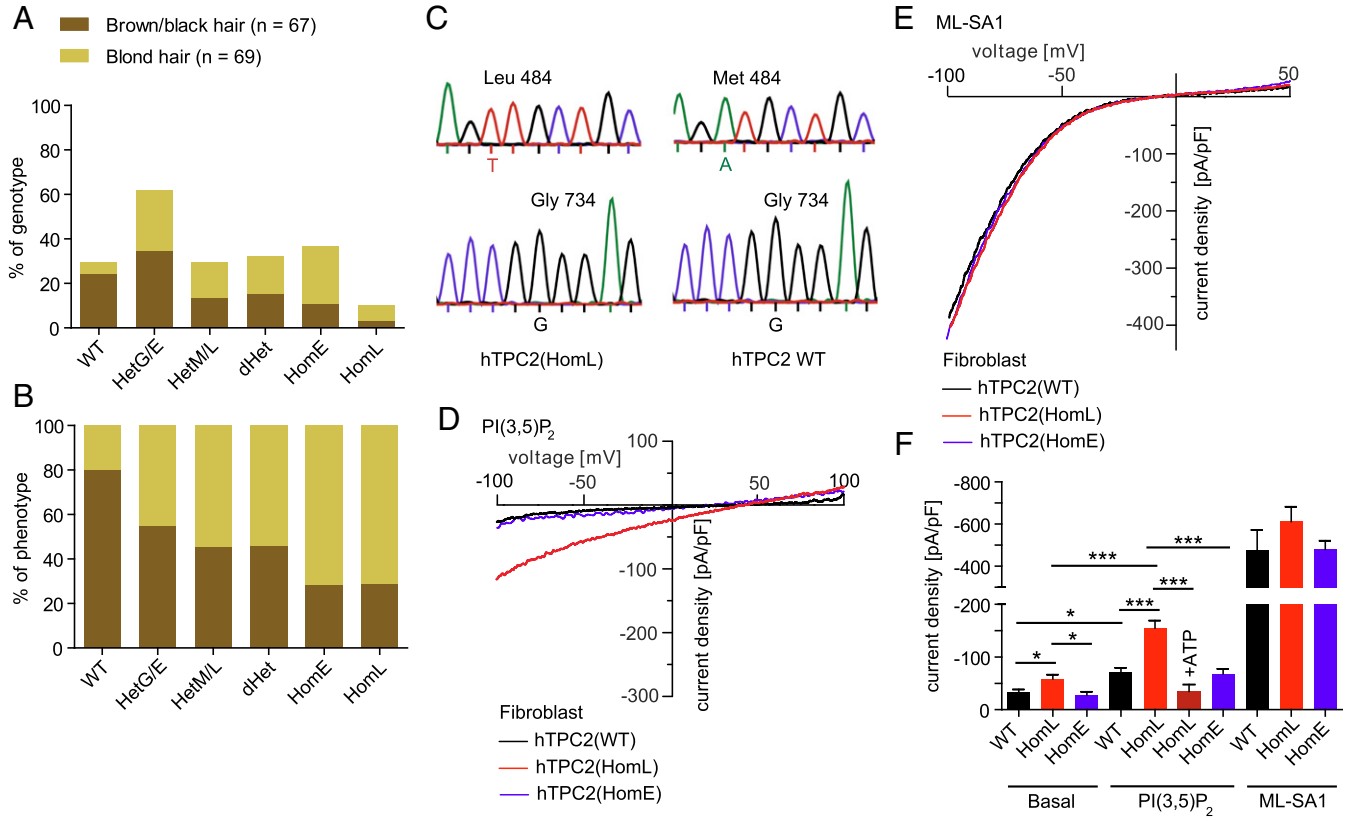

Fig. 5. Characterization of human fibroblasts isolated from TPC2 WT donors or donors carrying TPC2 polymorphisms. (*A* and *B*) Data summarizing sequencing results obtained from human genomic DNA samples. Shown in *A* is the genotype distribution (in percent) of individuals with either blond hair or brown/black hair (e.g., 23.9% of the brown/black hair donors but only 5.8% of the blond hair donors are genotype WT). In contrast, 26.1% of the blond hair donors are homozygous for E (homE) at position 734 while only 10.4% of the brown/black hair donors are homE. Shown in *B* is the phenotype distribution (in percent) of all genotyped individuals (e.g., 80% of all individuals with the genotype WT have brown/black hair while only 20% have blond hair). In contrast, 72% of all individuals with the genotype homE at position 734 and 71.4% of all individuals with the genotype L homozygous (homL) at position 484 are blond. The total numbers of donors were 67 (brown/black hair) and 69 (blond hair), respectively. (*C*) Examples of human donor genotyping results. Shown are respective sequences around position 484 (Leu/Met) and 734 (Gly). (*D* and *E*) Representative endolysosomal patch-clamp experiments showing $PI(3,5)P_2$ (10 μM) activated currents in vacuolin-enlarged fibroblast endolysosomes isolated from donors homozygous for WT, M484L, and G734E. The TRPML channel activator ML-SA1 was used to demonstrate that TRPML currents were comparable in size in all fibroblast lines, in contrast to $PI(3,5)P_2$-mediated currents. (*F*) Statistical summary of data shown in D and *E*. Two independent donor fibroblast samples were used for each WT and M484L. One sample was used for G734E. Shown are the pooled average current densities at −100 mV of at least five independent experiments, each. To test for statistical significance one-way ANOVA test followed by Tukey's posttest was applied. ***$P < 0.001$, *$P < 0.05$.

potency of $PI(3,5)P_2$, inhibition of channel activity by ATP was less sensitive in G734E compared with WT (*SI Appendix*, Fig. S6). The M484L polymorphism leads to structural changes affecting the pore diameter of TPC2. Thus, M484L displays a significant pore dilation compared with WT as demonstrated by molecular dynamics simulations and ion substitution experiments. The G734E variant is less responsive to ATP and more sensitive to mTOR inhibitors than WT, the latter suggesting that the weaker ATP effect may be mediated by mTOR. While torin-1 is a selective ATP-competitive inhibitor of mTOR which effectively blocks phosphorylation of mTOR, rapamycin and related inhibitors form a complex with the intracellular immunophilin FKBP12; the resulting complex then interacts with and inhibits mTOR (19, 20). Despite these different mTOR inhibitory mechanisms, both torin-1 and rapamycin result in a stronger increase in G734E activity compared with WT, further emphasizing that the differences in ATP block may be directly mediated via mTOR and downstream effects. Nevertheless, we cannot fully exclude the possibility of mTOR-independent ATP effects.

Remarkably, human TPC2 cDNAs used for functional studies in past publications were often polymorphic variants. For example, Calcraft et al. (21) had used a TPC2 variant cloned from HEK293 cells containing both polymorphisms: M484L and G734E. Pitt et al. (22) had used a variant of human TPC2 containing the G734E polymorphism (GenBank accession no. AY029200) and Brailoiu et al. (23) had used the IMAGE clone 5214862 (GenBank accession no. BC063008) which also contains the polymorphism G734E. Thus, it seems that WT hTPC2, at least in its recombinant form, has not always been used as a reference in the existing publications.

In accordance with recent findings by Ambrosio et al. (11) as well as Bellono et al. (12), claiming that loss of TPC2 leads to increased melanin production, an increase in TPC2 channel activity as found here for the two SNPs would be expected to result in the opposite effect, a decrease in melanin production. Located in the basal epidermis and in hair follicles, melanocytes of the integument are responsible for hair coloration through production of melanin pigments in melanosomes (24). Two types of pigment are known to give hair its color: eumelanin and pheomelanin. Eumelanin has two subtypes, black and brown, which determine the darkness of the hair color. A low concentration of brown eumelanin results in blond hair, whereas a higher concentration of eumelanin will color the hair brown/black. Melanin production is strongly dependent on the activity of the enzyme tyrosinase (TYR). TYR activity is optimal at neutral pH (25–27). To achieve neutralization of melanosomal pH, the proper function of a cascade of ion transporters seems to be required (27). Consequently, polymorphisms in any of such transporters or ion channels rendering them dys- or malfunctional may lead to changes in melanosome pH and thus to changes in melanin production, as suggested recently by Ito and Wakamatsu (27). For TPC2 this hypothesis has now been supported by works published by Ambrosio et al. (11) and Bellono et al. (12). Thus, loss of TPC2 leads to an increase in melanosomal pH and melanin production while overexpression of TPC2 leads to a decrease in melanin production. Like TPC2 overexpression, an increase in TPC2 activity would be expected to result in a decreased melanosomal pH and thus a decrease in melanin production. This would consequently explain the shift in hair color from brown to blond.

In addition to hair coloration, altered TPC2 channel activity may also impact human health, in particular under challenging conditions such as physical stress or infections. TPC2 knockout mice show an increased susceptibility to hypercholesterinemia and fatty liver hepatitis compared with WT when fed with a high-cholesterol diet (2), they show a decreased physical endurance under fasting conditions (3), and they are less susceptible to distinct viral infections (7). Migration of cancer cells and the formation of metastases was recently found to be reduced in TPC2 knockdown cells or after pharmacological inhibition of TPC2 (9). We therefore speculate that humans carrying the GOF polymorphisms M484L or G734E, or both, may have, in particular under stress conditions, an altered susceptibility for diseases that are associated with the endolysosomal system. In addition, it may also be possible that changes in TPC2 activity affect melanosomes differently than lysosomes, for example due to differences in pH regulatory mechanisms with different consequences for human physiology and pathophysiology.

Materials and Methods

Molecular Biology. All human TPC2 variants were generated from hTPC2(M484L/G734E)-mCherry, a gift from Michael Zhu, University of Texas Medical School, Houston. Point mutations were removed from constructs by site-directed mutagenesis using QuikChange (Agilent) according to the procedures outlined in the manufacturer's manual or by overlap PCR experimentation. C-terminally fused YFP versions of WT and the polymorphic TPC2 variants were generated from the respective mCherry constructs and subcloned into pcDNA3.1 vector. Constructs used for FRET experiments are described in *Materials and Methods* and the figure legends in more detail.

Endolysosomal Membrane Preparations. To evaluate expression levels of TPC2 WT and variants in endolysosomal membranes, HEK293 cells were transfected with TPC2-constructs (YFP-tagged), respectively. Preparation of endolysosomes was performed as described previously (17, 28). For immunoblotting, antibodies were used in the following dilutions: rabbit anti-Rab7, 1:500 (2094S; cell signaling); mouse anti-GFP, 1:2,000; mouse anti-HRP 1:2,000 (sc-2031; Santa Cruz); and rabbit anti HRP, 1:1,000 (NA934V; GE Healthcare).

Molecular Modeling. A model for TPC2 was constructed using Schrödinger Prime based on Protein Data Bank ID code 5E1J (14) with the UniProt sequence Q8NHX9 (21). Default settings were used using the multichain protocol modeling both subunits simultaneously. Always two of the resulting models were embedded into a 1-palmitoyl-2-oleoyl-*sn*-glycero-3-phosphocholine (POPC) bilayer in antiparallel orientation to reduce lateral stress following protocols described earlier (29, 30) and solvated with simple point charge water. $CaCl_2$ was added to balance the overall charge and to achieve nearly physiological ion concentrations. Using GROMACS-5.1 the periodic system was energy-minimized and constraints on the protein were gradually reduced (31–33). A total of 100 ns each were simulated with a time step of 2 fs for the WT, WT with $PI(3,5)P_2$, M484L, and M484L with $PI(3,5)P_2$. Two equivalents per pore were placed in the vicinity of M484L into the bilayer for the corresponding simulations. Neighbor searching was performed every 40 steps. The particle mesh Ewald algorithm was used for electrostatic interactions with a cutoff of 1.2 nm and Verlet cutoff scheme. A reciprocal grid of $192 \times 120 \times 120$ cells was used with fourth-order B-spline interpolation. A single cutoff of 1.2 was used for van der Waals interactions. Temperature coupling to 310 K was done with the V-rescale algorithm. Semiisotropic pressure coupling to 1 bar in the plane and perpendicular to it was done with the Berendsen algorithm. For all simulations the 53a6 force field was used with parameters for POPC adapted from ref. 29 and adapted for $PI(3,5)P_2$ from ref. 34. The analysis was performed using GROMACS tools, VMD, Schrödinger, and hole2 (31, 35–37).

FRET Experiments. Measurements of single-cell FRET based on aggregate (nonspatial) fluorescence recordings were performed and analyzed using the three-cube FRET method as described previously (38). For measurements, transiently transfected HEK293 cells were maintained in buffer solution composed of 140 mM NaCl, 5 mM KCl, 1 mM $MgCl_2$, 2 mM $CaCl_2$, 10 mM glucose, and 10 mM Na-Hepes, pH 7.4, at room temperature (RT). Fluorescence intensities of YFP or the GFP variants Citrine and Cerulean were recorded using a LEICA DMI6000B inverted epifluorescence microscope and a photomultiplier detection system (PTI). Excitation was done at 436 nm ± 2.5 or 500 nm ± 2.5 with a DeltaRam monochromator (Horiba). Epifluorescence emission was detected by a photomultiplier (PMT 914) and acquired on a personal computer using FelixGX software (Horiba). Three-cube FRET filter cubes were as follows (excitation; longpass beamsplitter; emission): CFP/Cerulean (ET436/20×; T455lp; ET480/40m), YFP/Citrine (ET500/20×; T515lp; ET535/30m), and FRET (ET436/20×; T455lp; ET535/30m) (Chrome Technology). The FRET ratio, which is defined as the fractional increase in YFP emission caused by FRET, was calculated using $FR = [SFRET - (R_D)(S_{Cer})]/[(R_A)(S_{Cit})]$. S_{FRET}, S_{Cer}, and S_{Cit} denote fluorescence intensities derived from measurements in individual cells coexpressing Citrine- or Cerulean-tagged proteins with the respective filter cube (excitation, emission): S_{FRET} (436 nm ± 10, 535 nm ± 15), S_{CFP} (436 nm ± 10, 480 nm ± 20), and, S_{YFP} (500 nm ± 10, 535 nm ± 15). R_D and R_A are experimentally predetermined constants from measurements applied to single cells expressing only Cerulean- or Citrine-tagged molecules that

correct for donor bleed through or acceptor cross-excitation. FRET efficiencies (E_A) can be calculated from FRs using the following equation (39):

$$E_A = [FR - 1] \cdot \frac{\varepsilon_{citrine}(436)}{\varepsilon_{cerulean}(436)}. \quad [1]$$

$\varepsilon_{citrine}$ and $\varepsilon_{cerulean}$ are the setup specific average molar extinction coefficients for citrine and cerulean, respectively, over the precise bandwidth of the FRET cube excitation filter. In our setup, the calculated molecular extinction coefficient ratio is $\varepsilon_{citrine}$ (436)/ $\varepsilon_{cerulean}$ (436) = 0.0563. Data were analyzed using FelixGX (Horiba PTI) and Microsoft Excel (Microsoft).

Whole-Endolysosomal Patch-Clamp Experiments. For whole-endolysosomal patch-clamp recordings, isolated intact endolysosomes from HEK293 cells were manually isolated after vacuolin treatment for at least 2 h. Human TPC2 WT and polymorphic TPC2 variants (C-terminally fused to YFP) were transiently transfected into HEK293 cells using TurboFect Transfection Reagent (ThermoFisher). Currents were recorded using an EPC-10 patch-clamp amplifier and PatchMaster acquisition software (HEKA). Data were digitized at 40 kHz and filtered at 2.8 kHz. Cytoplasmic solution contained 140 mM potassium methanesulfonate (KMSA), 5 mM KOH, 4 mM NaCl, 0.39 mM $CaCl_2$, 1 mM EGTA, and 20 mM Hepes (pH adjusted with KOH to 7.2). Luminal solution was 140 mM NaMSA, 5 mM KMSA, 2 mM CaMSA, 1 mM $CaCl_2$, 10 mM Hepes, and 10 mM MES (pH adjusted with MSA to 4.6). For the application of $PI(3,5)P_2$ (A.G. Scientific) and ATP-Mg (Sigma), cytoplasmic solution was completely exchanged by compound containing solution. Torin-1 and rapamycin were purchased from Tocris and LC Laboratories, respectively. All recordings were performed at 23–25 °C. For experiments using ATP and mTOR inhibitors, cell density was 50–60% and the time spent outside the incubator was 30 min.

To estimate the pore diameter of TPC2 WT and M484L, the relative permeability ratios of cations relative to Na^+ were plotted against the diameter of the respective monovalent cations as indicated in Fig. 4. The following equation was applied (40):

$$\frac{P_{X^+}}{P_{Na^+}} = k\left(1 - \frac{a}{d}\right)^2, \quad [2]$$

where a is the diameter of the permeating cation, k is a constant factor, and d is the pore diameter (41). The ionic radii of Li^+, K^+, Rb^+, and Cs^+ are 0.6, 1.33, 1.48, and 1.69 Å, respectively (42). To calculate the permeability ratios the following equation was used:

$$\frac{P_{X^+}}{P_{Na^+}} = \frac{[Na]_i}{[X^+]_o} e^{\frac{VF}{RT}}, \quad [3]$$

where V is the reversal potential, R is the gas constant, F is the Faraday constant, and T is the temperature in Kelvin. To determine the relative Na^+ ($P_X{}^+/P_{Na}{}^+$) permeabilities of TPC2 WT and M484L, whole-endolysosome recordings were performed using ramp protocols (+100 to −100 mV with 500-ms increments). The bath solution contained 160 mM (pH 7.2, Hepes 5 mM) of the respective cations (Fig. 4 *A*–*D*) and the pipette solutions contained 160 mM NaCl (pH 7.2, Hepes 5 mM). The recordings were started with symmetric Na^+ solutions. The cytoplasmic solution was then exchanged with the respective monovalent cation-containing solution.

Human Donor DNA Purification and Sequencing. Human genomic DNA was obtained from adult male and female individuals using the Gentra Puregene Buccal Cell Kit (Qiagen), according to manufacturer's instructions. Briefly, buccal cells were collected by scraping the inside of the mouth 10 times. For cell lysis, the collection brush was incubated in lysis solution at 65 °C for at least 15 min. Proteins were precipitated and centrifuged. To precipitate DNA, the supernatant was added to isopropanol and glycogen solution. The pellet was washed with 70% ethanol and air-dried before resuspension in DNA hydration solution. Samples were incubated at 65 °C for 1 h, followed by incubation at RT overnight to dissolve the DNA. Genomic DNA fragments were amplified using gene-specific primers [hTPC2(M484L) genomic DNA-forward: 5′-GGTGTTCCTGGTGCTGGA-3′; hTPC2(M484L) genomic DNA-reverse: 5′-ACAGCCTCTAGTCCTCAGGG-3′; hTPC2(G734E) genomic DNA-forward: 5′-GGCCACCTACCAGATGACT-3′; hTPC2(G734E) genomic DNA-reverse: 5′-CGGACGTCACCTGCACAG-3′]. All DNA sequencing services were done by Eurofins MWG Operon.

Isolation of Human Fibroblasts. Human genomic DNA sampling and human fibroblast isolation were approved by the Ludwig-Maximilians-Universität Ethics Committee (headed by Prof. Dr. Eisenmenger; reference no. 254–16). Acquisition of human material was performed after obtaining written informed consent by the donors. Primary fibroblasts were isolated by Prof. Dr. Carola Berking and colleagues, Department of Dermatology, Ludwig-Maximilians-Universität München from the skin of healthy adult donors. Epidermis was separated from dermis using dispase II (10 mg/mL in PBS, pH 7.2–7.4, D4693; Sigma) and dermis was digested in collagenase (1 mg/mL in DMEM, C0130; Sigma) for 22 h at room temperature. Fibroblasts were cultured in DMEM with glutamine (Life Technologies, Inc.) and 10% FBS (FBS Superior, S0615; Biochrom). They were used for experiments at passages three to seven.

Statistical Analysis. Details of statistical analyses and n values are provided in the *Materials and Methods* or the figure legends. Statistical analyses were carried out using Origin 7.5 and GraphPad Prism 5. All error bars are depicted as mean ± SEM. Significance is denoted on figures as outlined in the legends. Statistics were derived from at least three independent experiments.

ACKNOWLEDGMENTS. We thank Kerstin Skokann, Melanie Wallisch, and Berit Noack (Ludwig-Maximilians-Universität München) for technical support; Dr. Bernd Schröder (University of Kiel) for kindly providing the human TMEM192 cDNA; and Dr. Michael Zhu (University of Texas Medical School at Houston) for kindly providing the human TPC2(M484L/G734E)-mCherry cDNA. This work was supported, in part, by German Research Foundation Grants SFB/TRR152 TP04 (to C.G.), TP06 (to C.A.W.-S.), and TP12 (to M.B.) and by funding from the Neuronal Ceroid Lipofuscinosis Foundation, Hamburg, Germany.

1. Favia A, et al. (2014) VEGF-induced neoangiogenesis is mediated by NAADP and two-pore channel-2-dependent Ca2+ signaling. *Proc Natl Acad Sci USA* 111:E4706–E4715.
2. Grimm C, et al. (2014) High susceptibility to fatty liver disease in two-pore channel 2-deficient mice. *Nat Commun* 5:4699.
3. Cang C, et al. (2013) mTOR regulates lysosomal ATP-sensitive two-pore Na(+) channels to adapt to metabolic state. *Cell* 152:778–790.
4. García-Rúa V, et al. (2016) Endolysosomal two-pore channels regulate autophagy in cardiomyocytes. *J Physiol* 594:3061–3077.
5. Lin PH, et al. (2015) Lysosomal two-pore channel subtype 2 (TPC2) regulates skeletal muscle autophagic signaling. *J Biol Chem* 290:3377–3389.
6. Arndt L, et al. (2014) NAADP and the two-pore channel protein 1 participate in the acrosome reaction in mammalian spermatozoa. *Mol Biol Cell* 25:948–964.
7. Sakurai Y, et al. (2015) Ebola virus. Two-pore channels control Ebola virus host cell entry and are drug targets for disease treatment. *Science* 347:995–998.
8. Ruas M, et al. (2010) Purified TPC isoforms form NAADP receptors with distinct roles for Ca(2+) signaling and endolysosomal trafficking. *Curr Biol* 20:703–709.
9. Nguyen ON, et al. (2017) Two-pore channel function is crucial for the migration of invasive cancer cells. *Cancer Res* 77:1427–1438.
10. Sulem P, et al. (2008) Two newly identified genetic determinants of pigmentation in Europeans. *Nat Genet* 40:835–837.
11. Ambrosio AL, Boyle JA, Aradi AE, Christian KA, Di Pietro SM (2016) TPC2 controls pigmentation by regulating melanosome pH and size. *Proc Natl Acad Sci USA* 113:5622–5627.
12. Bellono NW, Escobar IE, Oancea E (2016) A melanosomal two-pore sodium channel regulates pigmentation. *Sci Rep* 6:26570.
13. Kintzer AF, Stroud RM (2016) Structure, inhibition and regulation of two-pore channel TPC1 from Arabidopsis thaliana. *Nature* 531:258–262.
14. Guo J, et al. (2016) Structure of the voltage-gated two-pore channel TPC1 from Arabidopsis thaliana. *Nature* 531:196–201.
15. Wang X, et al. (2012) TPC proteins are phosphoinositide- activated sodium-selective ion channels in endosomes and lysosomes. *Cell* 151:372–383.
16. Perl A (2015) mTOR activation is a biomarker and a central pathway to autoimmune disorders, cancer, obesity, and aging. *Ann N Y Acad Sci* 1346:33–44.
17. Schieder M, Rötzer K, Brüggemann A, Biel M, Wahl-Schott C (2010) Planar patch clamp approach to characterize ionic currents from intact lysosomes. *Sci Signal* 3:pl3.
18. Shen D, et al. (2012) Lipid storage disorders block lysosomal trafficking by inhibiting a TRP channel and lysosomal calcium release. *Nat Commun* 3:731.
19. Faivre S, Kroemer G, Raymond E (2006) Current development of mTOR inhibitors as anticancer agents. *Nat Rev Drug Discov* 5:671–688.
20. Hausch F, Kozany C, Theodoropoulou M, Fabian AK (2013) FKBPs and the Akt/mTOR pathway. *Cell Cycle* 12:2366–2370.
21. Calcraft PJ, et al. (2009) NAADP mobilizes calcium from acidic organelles through two-pore channels. *Nature* 459:596–600.
22. Pitt SJ, et al. (2010) TPC2 is a novel NAADP-sensitive Ca2+ release channel, operating as a dual sensor of luminal pH and Ca2+. *J Biol Chem* 285:35039–35046.
23. Brailoiu E, et al. (2009) Essential requirement for two-pore channel 1 in NAADP-mediated calcium signaling. *J Cell Biol* 186:201–209.
24. Borges CR, Roberts JC, Wilkins DG, Rollins DE (2001) Relationship of melanin degradation products to actual melanin content: Application to human hair. *Anal Biochem* 290:116–125.

25. Ancans J, et al. (2001) Melanosomal pH controls rate of melanogenesis, eumelanin/phaeomelanin ratio and melanosome maturation in melanocytes and melanoma cells. *Exp Cell Res* 268:26–35.
26. Smith DR, Spaulding DT, Glenn HM, Fuller BB (2004) The relationship between Na(+)/H(+) exchanger expression and tyrosinase activity in human melanocytes. *Exp Cell Res* 298:521–534.
27. Ito S, Wakamatsu K (2011) Human hair melanins: What we have learned and have not learned from mouse coat color pigmentation. *Pigment Cell Melanoma Res* 24:63–74.
28. Chen CC, et al. (2014) A small molecule restores function to TRPML1 mutant isoforms responsible for mucolipidosis type IV. *Nat Commun* 5:4681.
29. Krüger J, Fischer WB (2008) Exploring the conformational space of Vpu from HIV-1: A versatile adaptable protein. *J Comput Chem* 29:2416–2424.
30. Sommer B, et al. (2011) CELLmicrocosmos 2.2 MembraneEditor: A modular interactive shape-based software approach to solve heterogeneous membrane packing problems. *J Chem Inf Model* 51:1165–1182.
31. Abraham MJ, et al. (2015) GROMACS: High performance molecular simulations through multi-level parallelism from laptops to supercomputers. *SoftwareX* 1:19–25.
32. Krüger J, Fischer WB (2010) Structural implications of mutations assessed by molecular dynamics: Vpu1-32 from HIV-1. *Eur Biophys J* 39:1069–1077.
33. Avbelj M, et al. (2014) Activation of lymphoma-associated MyD88 mutations via allostery-induced TIR-domain oligomerization. *Blood* 124:3896–3904.
34. Holdbrook DA, et al. (2010) Stability and membrane orientation of the fukutin transmembrane domain: A combined multiscale molecular dynamics and circular dichroism study. *Biochemistry* 49:10796–10802.
35. Humphrey W, Dalke A, Schulten K (1996) VMD: Visual molecular dynamics. *J Mol Graph* 14:33–38.
36. Jacobson MP, et al. (2004) A hierarchical approach to all-atom protein loop prediction. *Proteins* 55:351–367.
37. Smart OS, Goodfellow JM, Wallace BA (1993) The pore dimensions of gramicidin A. *Biophys J* 65:2455–2460.
38. Butz ES, et al. (2016) Quantifying macromolecular interactions in living cells using FRET two-hybrid assays. *Nat Protoc* 11:2470–2498.
39. Nguyen ON, et al. (2016) Peripherin-2 differentially interacts with cone opsins in outer segments of cone photoreceptors. *Hum Mol Genet* 25:2367–2377.
40. Owsianik G, Talavera K, Voets T, Nilius B (2006) Permeation and selectivity of TRP channels. *Annu Rev Physiol* 68:685–717.
41. Bormann J, Hamill OP, Sakmann B (1987) Mechanism of anion permeation through channels gated by glycine and gamma-aminobutyric acid in mouse cultured spinal neurones. *J Physiol* 385:243–286.
42. Robinson RA, Stokes RH (2002) *Electrolyte Solutions: Second Revised Edition* (Dover, Mineola, NY), 2nd Ed.